ARTICLE NO. 78-681

12-cm Argon/Xenon Ion Source

W.D. Ramsey*
Xerox Electro-Optical Systems, Pasadena, Calif.

The original 12-cm hexagonal magneto-electrostatic containment discharge chamber described by Moore in 1969 has been optimized for argon and xenon operation. Argon mass utilization efficiencies of 67-80% were achieved at keeper-plus-main discharge energy consumptions of 200-458 eV/ion, respectively. Xenon performance of 85-96% mass utilization was realized at 200-350 eV/ion. The paper discusses the optimization process and test results.

Introduction

THE operational hypothesis of the magneto-electrostatic containment (MESC) design was first derived by R. David Moore[1] in 1969. He showed that a particular array of permanent magnets and strip anodes would minimize ionic wall recombination (Fig. 1).

This concept was applied to the fabrication of a 12-cm, hexagonal discharge chamber. Cesium operational tests produced excellent performance with high mass utilization efficiency and exceptionally low ionization discharge energy consumption. Subsequently, the same discharge chamber was modified for mercury operation by design changes in the cathode subassembly and boundary anodes.[2]

The following discussion describes the conversion of the same 12-cm hexagonal discharge chamber from mercury-to-argon/xenon operation. The discussion includes a description of the test facility, feed system, optimization process and test results.

Test Setup

Vacuum Facility

Tests were conducted in a 1.5×3.6 m vacuum system. Six 25-cm diameter oil diffusion pumps with a combined pumping speed of 24,000 l/s were used to evacuate the chamber. Vacuum chamber pressure was found to vary both with mass flow and the gas being tested. A chamber pressure of 4.0×10^{-5} Torr was maintained with 1.0 A equivalent flow of argon or 0.400 A flow of xenon.

Feed System

Propellant gases were provided by the laboratory feed system, shown in Fig. 2. The system could be rapidly changed from argon to xenon operation. The system could also be configured for mixed mode with argon main flow and xenon cathode.

Approximate flow measurements were taken from the rotometers and precision readings from a mass flow transducer. The tapered bore rotometers were capable of measuring gas flows to an accuracy of 0.21 ml/min under ideal conditions. The mass flow transducer had an accuracy of 0.1 ml/min with up to 20% variation in temperature and pressure. Test gas was fed into the discharge chamber through two needle valves that controlled flow to the hollow cathode[2] and main feed ring.[1]

Presented as Paper 78-681 at the AIAA/DGLR 13th International Electric Propulsion Conference, San Diego, Calif., April 25-27, 1978; submitted May 15, 1978; revision received Nov. 7, 1978.

Index category: Electric and Advanced Space Propulsion.

*Physicist. Member AIAA.

Cathode Subassembly

The cathode subassembly was a set of concentric tubes with a 3.2-mm hollow cathode on axis. The tubes were made of different material and were used to heat shield, electrically isolate, and support the keeper electrode and baffle disk (Fig. 3).

The cathodes had orifice diameters that ranged from 0.46 to 0.61 mm to test argon/xenon operational characteristics.[3] These cathodes used a porous tungsten-impregnated tubular emitter 2.54 cm long located against the upstream face of the orifice plate.[4]

The keeper electrode was a ring of 1.0-mm diameter tantalum wire 1.5 mm downstream of the cathode orifice plate. It was supported with four wires spotwelded to the keeper tube.

The 1.54-cm diameter 300 series stainless steel baffle tube provided baffle disk support. The disk was supported by four wires spotwelded to the inside diameter of the tube.

The baffle tube was connected to a vacuum penetration control rod. Rod movement produced 2.5-cm tube axial motion.

Electrodes

A recent report by Aston[5] showed that a reduction in accel grid transparency would reduce the neutral flux leaving the discharge chamber and increase the ionization probability. To take advantage of this, small-hole accel grid (SHAG) optics were designed and used for testing. The hydroformed grids were fabricated from 0.25-mm thick molybdenum dished 5.1 mm downstream at the center. Screen and accel holes were located on 2.53-mm centers in a hexagonal close pattern of 2269 holes of 2.24- and 1.17-mm diameter. This design produced grid geometric transparencies of approximately 70 and 20%.

Experimental Approach

Ion source optimization was accomplished by varying source operational parameters in a systematic manner. Data from each test were reviewed and the information used to reconfigure boundary anodes and cathode baffle geometry.

The original derivation of the MESC concept[1] showed discharge plasma boundary-diffusion current was a function of chamber geometry and plasma operational parameters. It was found to be directly proportional to the square of the plasma density and inversely proportional to the square of the magnetic field across the boundary anodes (B_0). This magnetic field could be varied by changing the boundary anode positions relative to the magnetic pole faces. The further the anodes are into the discharge chamber, the less the field strength.

Tests usually followed the same rough outline with data recorded between each operational parameter change. Once the gas flow was confirmed to be stable at a convenient level, the baffle assembly was adjusted for maximum arc current.

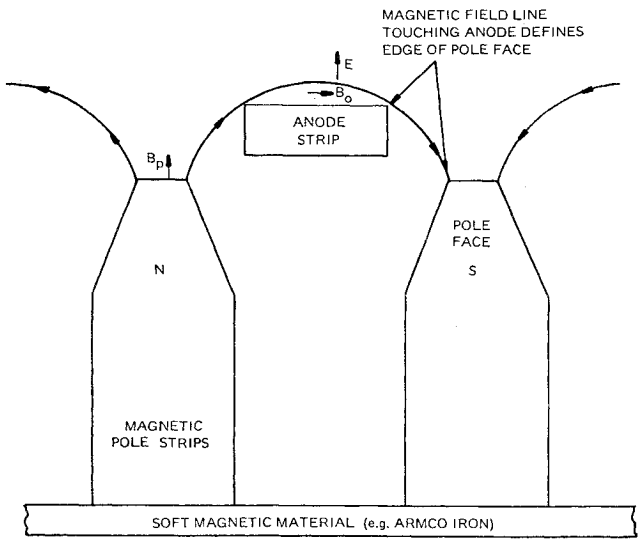

Fig. 1 Magneto-electrostatic containment geometry.

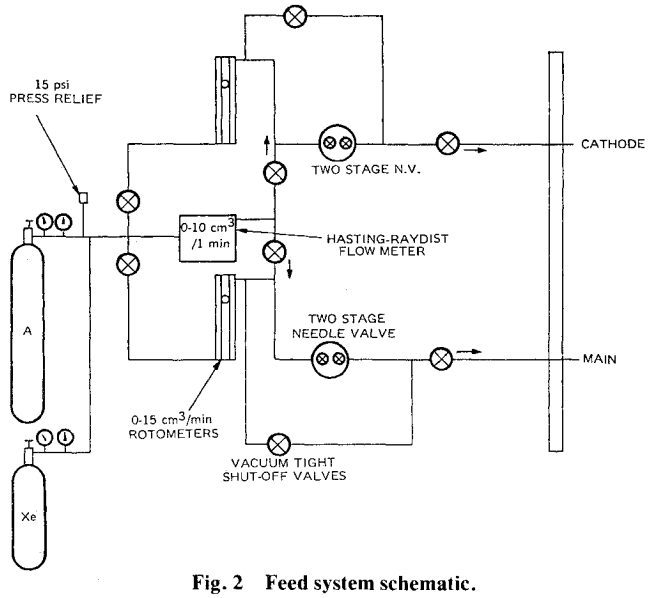

Fig. 2 Feed system schematic.

Next, the arc potential was varied in a stepwise manner from the lowest stable potential to at least 10 V above the operational nominal. If mass utilization efficiency was high and the arc impedance within the nominal range, further data were collected. If not, the cathode/main feed flow ratio was changed and the procedure repeated. Measurements were repeated at least three times at three different total mass flows for each boundary anode, and baffle configuration, and gas tested.

Test Results

During argon, xenon, and "mixed mode" operation, 80, 96, and 76% mass utilization efficiencies were achieved at 458, 350, and 342 eV/ion, respectively, as can be seen in Fig. 4 and Tables 1 and 2. In mixed-mode operation, different gases were fed into the discharge through the cathode and main feed. Argon flowed through the anode potential main feed ring and xenon through the cathode.

Test data were corrected for backstreaming neutral flux and double-charged ion in computing the ion source performance results presented in Fig. 4 and Tables 1 and 2. Backstreaming flux was calculated from the kinetic theory of gases[6] and added to the total mass flow in finding the corrected mass utilization efficiency.

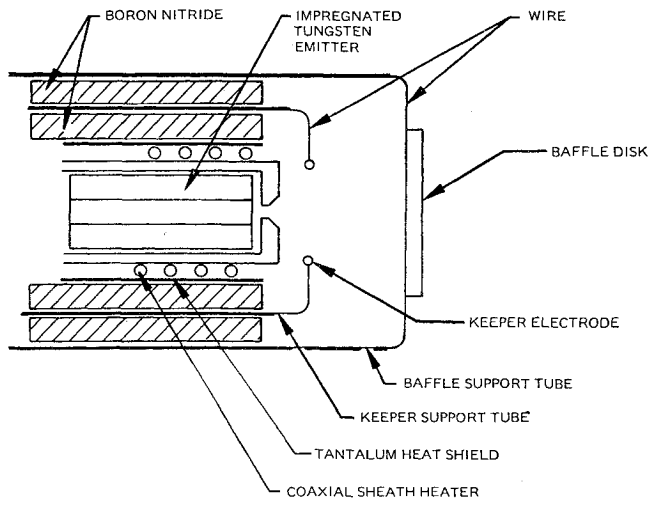

Fig. 3 Hollow cathode subassembly.

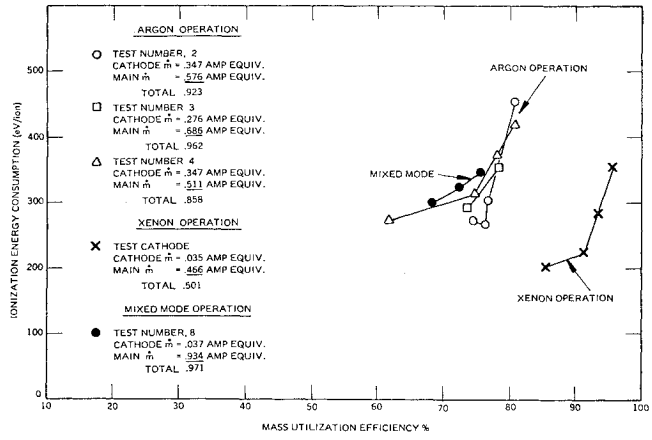

Fig. 4 Ionization energy consumption vs mass utilization efficiency.

The percentages of double-charged ion current in the exhaust beam shown in Tables 1 and 2 were taken from time-of-flight data collected during the indicated tests. These results were found to be in good agreement with the arc potential vs double-charged ion percentages reported previously by Byers and Reader.[7]

One half of the calculated double-charged current was subtracted from the beam in computing ion source energy per ion and mass utilization efficiencies. These quantities represent the equivalent single-charged ion beam performance of the ion source.

As the tables show, mixed-mode data replicated argon test results in serveral ways. Best performance was obtained with 0.035 A equivalent xenon flow through the cathode and 0.934 A argon main feed.

Three distinct cathode operational modes were observed as a function of xenon gas flow. The high gas flow, 0.050 A equivalent, was characterized by low efficiency, high main discharge impedance, and high applied potential discharge operation. Discharge potentials of over 60 V were necessary to ionize 10-13% of the total mass flow in a 50Ω-discharge. Changes in the argon flow rate had no effect on the beam level.

Argon-like source performance was observed with xenon cathode flows ranging from 0.015 to 0.040 A equivalent. In this mode 47-60 V discharge potentials ionized 65-76% of the total mass flow in a 10-15 Ω plasma.

Classic cathode keeper "plume" mode operation was observed at a lower cathode xenon flow rates.

Table 1 Argon operation

Test no.	H.V.$^+$ V	J^+ A	H.V.$^-$ V	J^- A	Arc Voltage V	Arc Current A	Keeper Voltage V	Keeper Current A	Cathode mass equiv. A	Total mass equiv. A	eV[a]/ion	eV[b]/ion	% double charged	Mass[c] eff.,%
					Chamber pressure 3.8×10^{-5} Torr – backstreaming neutral ingestion 0.030 A equivalent									
	1100	.742	400	.011	47	4.20	8.2	0.25	.374	.984	272.	279.	4.6	70.4
	1200	.760		.011	47	4.50	8.0	0.25			285.	291.	4.6	72.2
1		.780		.011	50	5.00	8.0	0.25			327.	337.	5.3	73.8
		.800		.014	52	5.50	7.0	0.25			366.	377.	5.6	75.3
		.800		.014	56	6.00	7.0	0.25			429.	444.	6.5	75.0
		.710		.011	45	3.00	9.0	0.25			196.	200.	4.0	67.6
					Chamber pressure 4.0×10^{-5} Torr – backstreaming neutral ingestion 0.034 A equivalent									
	1200	.760	380	.012	52	3.6	14.5	0.500	.347	.923	259.	266.	4.8	76.3
		.770		.015	54	4.0	14.5	0.500			295.	303.	5.36	76.8
2		.820		.017	60	5.8	12.0	0.500			440.	458.	7.5	80.8
		.740		.011	52	3.7	13.0	0.500			273.	280.	4.8	74.3
	1200	.760	400	.014	49	4.2	12.5	0.500	.276	.962	284.	290.	4.0	73.2
3		.820		.015	55	4.9	10.0	0.500			341.	351.	5.71	78.3
		.760		.014	50	4.10	12.5	0.500			283.	289.	4.2	73.1
					Chamber pressure 2.5×10^{-5} Torr – backstreaming neutral ingestion 0.022 A									
	1000	.685	380	.010	49	4.11	13.0	0.50	.347	.858	308.	316.	5.0	74.8
		.685	380	.010	49	4.11	13.0				309.	316.	5.0	74.8
		.720		.012	55	4.55	13.0				362.	374.	6.2	78.0
4		.725		.011	55	4.50	12.0				355.	366.	6.2	78.6
		.750		.011	60	4.91	12.0				406.	423.	7.5	80.8
		.560		.008	45	3.20	13.0				273.	278.	4.0	61.5
		.685		.010	50	4.0	13.0	0.50			306.	315.	5.3	74.7
					Mixed-mode operation									
	1150	.715	380	.010	51	3.85	15.5	0.50	0.37	.971	289.	298.	5.5	68.5
8	1150	.760	380	.011	55	4.10	15.0	0.50			311.	321.	6.2	72.5
	1150	.795	380	.014	60	4.20	16.0	0.50			332.	342.	7.5	75.9

[a] Discharge and keeper ionization energy uncorrected for doubly ionized beam.
[b] Discharge and keeper ionization energy corrected for doubly ionized beam (equivalent single-charged performance).
[c] Mass efficiency corrected for doubly ionized beam (equivalent single-charged performance).

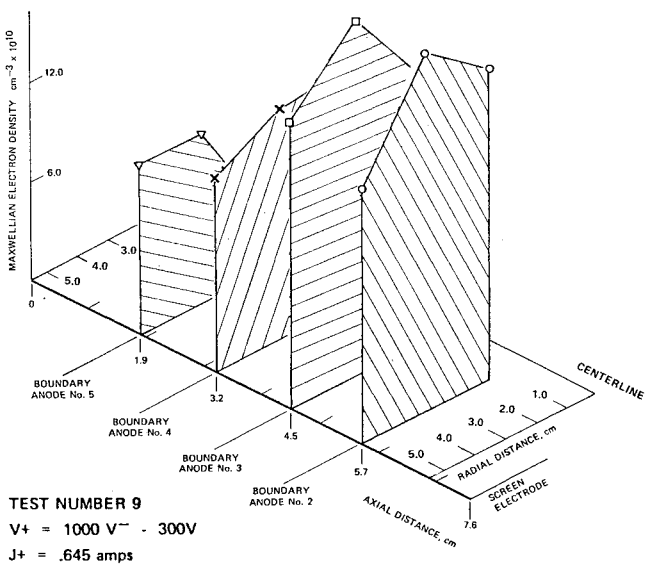

TEST NUMBER 9
V+ = 1000 V⁻ - 300V
J+ = .645 amps
△V = 53 volts
J_{arc} = 3.5 amp
Keeper Potential = 17V

Fig. 5 Maxwellian distribution 53 V discharge.

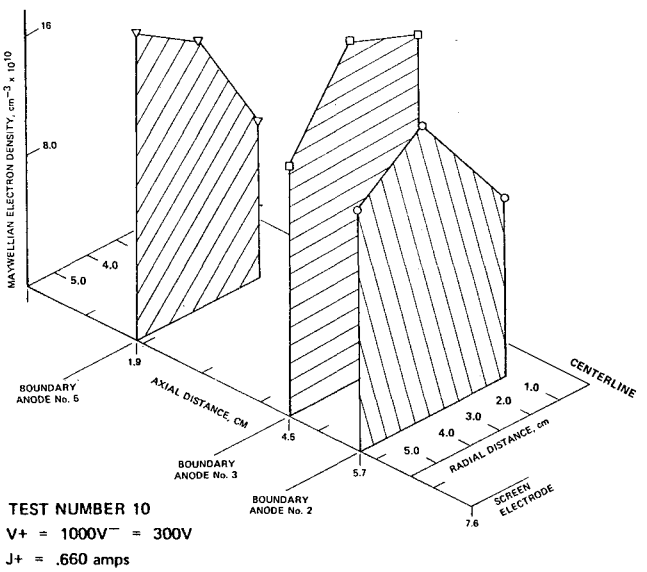

TEST NUMBER 10
V+ = 1000V⁻ = 300V
J+ = .660 amps
△V = 47 volts
J_{arc} = 4.5 amps
Keeper Potential = 12V

Fig. 6 Maxwellian distribution 47 V discharge.

Table 2 Xenon operation

Test no.	H.V.+ V	J+ A	H.V.− V	J− A	Arc Voltage V	Arc Current A	Keeper Voltage V	Keeper Current A	Cathode mass equiv. A	Total Mass equiv. A	eV[a]/ion	eV[b]/ion	% double charged	Mass[c] eff.,%
					Chamber pressure 6.2×10^{-5} T – backstreaming neutral ingestion 0.0426 A equivalent									
	1100	.490	320	.006	42	2.5	11.0	0.250	.035	.481	222.	225.	2.2	91.4
	1100	.510	320	.009	44	3.1	9.0	0.260	.035		276.	284.	4.7	93.4
5	1100	.540	500	.010	49	3.6	9.0	0.260	.035		337.	356.	10.8	95.8
	1100	.455	300	.006	40	2.2	11.5	0.250	.035		202.	203.	1.0	85.3
					Chamber pressure 6.6×10^{-5} T – backstreaming neutral ingestion 0.045 A equivalent									
	1200	.660	600	0.14	40	4.0	11.0	0.300	.037	.634	253.	254.	6.0	95.7
		.685		0.15	45	4.3	10.0	0.300			293.	302.	6.0	95.7
6		.710		.016	50	4.5	9.0	0.300			329.	350.	12.0	96.1
		.610		.012	37	3.6	12.0	0.300			228.	228.	0.0	88.1
		.640		.012	40	4.0	11.5	0.300			260.	261.	1.0	92.0
	1080	.635	600	.014	39	4.0	11.0	0.300			256.	257.	0.0	91.5
					Chamber pressure 2.5×10^{-5} T – backstreaming neutral ingestion 0.017 A equivalent									
	640	.300	300	.005	43	2.2	16.0	0.300	.043	.312	336.	343.	3.5	88.1
		.300		.006	45	2.5	16.0	0.300	.043	.312	399.	411.	6.0	86.7
7		.307		.010	48	4.15	10.0	0.300	.043	.312	680.	716.	9.6	85.9
	800	.280	300	.005	40	1.85	11.5	0.300			281.	283.	1.0	83.2
	600	.300	600	.008	43	3.20	11.0	0.300	.043	.312	482.	491.	3.5	87.2

[a] Discharge and keeper ionization energy uncorrected for doubly ionized beam.
[b] Discharge and keeper ionization energy corrected for doubly ionized beam (equivalent single-charged performance).
[c] Mass efficiency corrected doubly ionized beam (equivalent single-charged performance).

Discharge Chamber Optimization

For purposes of discussion the boundary anodes can be divided into two groups, six along the chamber side walls and three on the rear wall. Anodes were numbered from the screen grid toward the rear wall and from the outer-to-inner anode on the rear wall. The anodes were wired so that the current to each could be measured separately.

Preliminary tests conducted with the anodes located in the mercury discharge position found variation in the current density from anode to anode. Anode no. 2 had a current density 1.44, 1.34, 1.75, and 6.6 times that of anodes 3 through 6, respectively. Also, it was found that anode current distribution could be controlled by the baffle assembly axial position. Baffle movement either way from optimum reduced the current density differences at the expense of mass utilization efficiency. Changes in the cathode gas flow rate failed to improve mass efficiency.

The majority of the tests were conducted with 0.61-mm orifice cathodes located 1.0 cm downstream of the discharge chamber rear wall boundary anodes. The 0.61-mm size was selected after preliminary tests found that cathode gas flow vs electron emission characteristics were unaffected by orifice diameter. The larger orifice cathodes tended to have longer-lived emitters as they operated cooler. The cathode axial position was found using the criterion described by Moore.[1]

Tests were conducted with baffle disk diameters of 0.95 to 1.25 cm and tube-to-disk gaps of 1.0 to 4.5 mm. Optimum performance was seen with a 1.11-mm baffle disk located 3.2 mm from the support tube face. The baffle was positioned 6.4 mm downstream of the cathode orifice plate.

Optimum source performance was realized with the cathode baffle structure at the optimum position and boundary anode current densities that did not exceed 1.3 to 1, exclusive of corner anodes, nos. 1, 6, and 7. These ratios were achieved by adjusting individual anodes. In the mercury discharge position, B_0, the magnetic field parallel to the discharge chamber axis at the anodes, averaged 270 G. In the optimum configuration, B_0 reduced in magnitude. The average field across anodes 2 through 5 was 223, 190, 163, and 143 G, respectively. B_0 was 220 G across the rear wall anodes.

Magnetic field measurements were taken at the anode center with a 3.2-mm diameter Hall current probe located in the middle of the 4.0-mm-wide anodes. The probe was jigged to move parallel to the chamber wall at right angles to the boundary anode structures.

The magnetic field configuration described above implies the existence of an axial discharge plasma density gradient. Using the MESC magnetic field-bulk plasma density relationship mentioned previously, the density would have to change from anode to anode. Plasma density ratios between anode no. 2 and anodes 3, 4, and 5 were calculated as 0.85, 0.73, and 0.64. Langmuir probe measurements, discussed in a later section, tend to support these calculations.

Langmuir Discharge Probe

The Langmuir probe was made from a swaged assembly composed of an outer tube or metal sheath, insulation material, and a center conductor. The sheath and insulation was stripped away from one end of the assembly so that a 2.0-mm length of the .25-mm conductor could be exposed to the discharge chamber plasma.

During probe operation the sheath was allowed to float at plasma potential and the conductor was connected to a dc power supply referenced to boundary anode potential. The chassis of the supply was tied to positive high voltage and was isolated from ground with a 1:1 transformer in the input line. Polarity and probe potential changes were made with insulated rods attached to the supply. Probe data were collected by changing the probe potential and recording the current readings. The probe was attached to a vacuum bulkhead control rod for positioning. Rod motion located the probe 1.22, 3.02, and 5.54 cm from the discharge chamber centerline in the plane of boundary anodes 2 through 5.

Table 3 Langmuir probe data

Test number = 9	Arc potential = 53V			Cathode $\dot{m}$ = 0.155 (A equiv.)						Main $\dot{m}$ = 0.752 (A equiv.)		
	Anode no.											
	2			3			4			5		
Displacement from centerline, cm	1.22	3.02	5.54	1.22	3.02	5.54	1.22	3.02	5.54	1.22	3.02	5.54
Electron parameters												
Primary energy, eV	47	47	45	47	47	46	48	38	40	41	41	45
Primary density, $\frac{\text{electron}}{\text{cm}^3} \times 10^{10}$	6.4	7.0	5.0	5.0	7.0	5.6	5.0	5.0	4.0	3.0	4.5	3.0
Maxwellian energy, eV	3.8	4.0	4.0	4.4	4.0	4.0	4.6	4.2	4.0	5.4	5.75	4.0
Maxwellian density, $\frac{\text{electron}}{\text{cm}^2} \times 10^{10}$	19.8	21.2	15.1	14.5	21.2	17.0	14.1	14.0	12.0	7.3	10.6	9.0
Ion density, $\frac{\text{ion}}{\text{cm}^3} \times 10^{10}$	26.2	28.2	20.1	19.5	28.2	22.6	19.1	19.0	16.0	10.3	15.1	12.0

Table 4 Langmuir probe data

Test number = 10	Arc potential = 47V			Cathode $\dot{m}$ = 0.212 (A equiv.)			Main $\dot{m}$ = 0.725 (A equiv.)		
	Anode no.								
	2			3			5		
Displacement from centerline, cm	1.22	3.02	5.54	1.22	3.02	5.54	1.22	3.02	5.54
Electron parameters									
Primary energy, eV	40	44	45	43	40	42	44	45	46
Primary density, $\frac{\text{electron}}{\text{cm}^3} \times 10^{10}$	5.2	5.6	4.7	6.3	1.7	4.8	3.7	5.1	6.0
Maxwellian energy, eV	3.45	3.0	3.8	3.2	3.3	3.4	3.0	3.0	2.8
Maxwellian density, $\frac{\text{electron}}{\text{cm}^3} \times 10^{10}$	15.6	18.2	14.3	20.3	21.0	14.8	12.6	17.5	18.2
Ion density, $\frac{\text{ion}}{\text{cm}^3} \times 10^{10}$	20.8	23.8	19.0	26.6	22.4	19.6	16.3	22.6	24.2

Probe current-voltage data were reduced using the method described by Strickfaden and Geiler.[8] Plasma characteristics calculated from a 53 V argon discharge are shown in Fig. 5 and Table 3. Plasma density in the plane of anode no. 2 can be seen to change by 23% between the center and edge of the discharge. The edge, 5.54 from the center line position, was directly upstream of the outermost electrode grid holes. Maximum plasma density in this anode plane occurred midway between the central and edge probe positions and was 108% of the central density.

Table 4 and Fig. 6 show the characteristics derived from probe data at a slightly greater cathode mass flow. Plasma impedance was reduced as well as the energy of the primary and Maxwellian electron populations.

The 53 V argon discharge probe data show fair agreement with the axial plasma gradient calculated from the anode magnetic field measurements. Average bulk plasma-density ratio between anode 2 and anodes 3, 4, and 5 was 0.94, 0.73, and 0.49, respectively. Magnetic field-bulk plasma relationship yielded 0.85, 0.73, and 0.64 for the same ratios.

Both low- and high-impedance main discharges had the same characteristics in that the plasma density in the central region was slightly lower than a point halfway between the centerline and the boundary anodes. This was partly confirmed with Faraday probe cup measurements of the exhaust. The exhaust beam peak current occurs at two points on either side of the beam centerline. The center-to-peak current was found to vary by a maximum of 8% during high-impedance operation which was in good agreement with the values seen in the discharge plasma-density profile of the same test.

Beam Probe Measurements

Three Faraday cup type probes were used to measure the ion beam distribution by traversing through the beam plasma at right angles to the ion source center line. The motor driven assembly had 75 cm of travel. Two probes crossed the beam axis 22 cm downstream of the accel grid while a third crossed at 30 cm. One of the two at 22 cm was a 28 × 0.44 cm slit probe. The other two were cylindrical probes with 1.27-cm orifices.

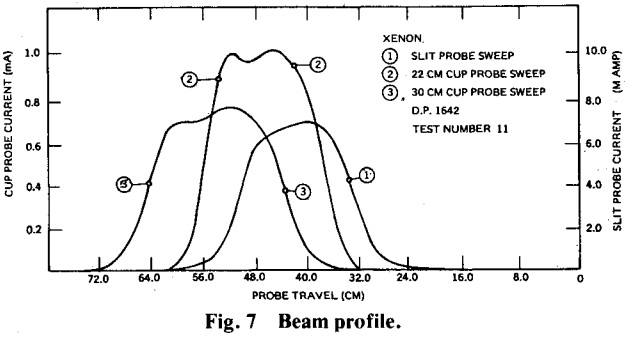

Fig. 7 Beam profile.

Beam width seen by the slit and cylindrical probe agreed on all data taken. However, the beam density distribution differed. Cylindrical probe data indicated the beam had a lower current density on axis that it did toward the edges. A typical cylindrical probe trace showed two maxima, one 2% greater than the other, with the central region of the beam 6% less than their average. A typical slit probe trace did not show a "hollow" beam but the current density did occur 4 deg off center in the same direction as the greater of the two maxima seen in the cylindrical probe trace, Fig. 7.

Beam flatness was calculated using the greatest current density collected and the total indicated ion current envelope width. A typical 0.400 A argon beam with screen and accel potentials of 800 and 400 V had a mean-to-maximum flatness ratio of 0.515 and 0.53 at 22 and 30 cm. Increasing the beam current to 0.649 A and the screen potential to 900 V increased the flatness to 0.576 and 0.585 for the near and far probes.

A 0.404 A xenon beam was found to have a flatness of 0.657 and 0.677 at the same downstream cross sections. The screen and accel potentials were 900 and 480 V, respectively.

Conclusion

The inert gas ion source tests demonstrated that the MESC discharge chamber design was capable of efficient operation with argon or xenon. Performance was achieved by optimizing boundary anode position and the baffle disk geometry in the existing 12-cm hexagonal discharge chamber. No attempts were made to optimize or change the basic design of the chamber. Comparing the cesium performance of this discharge chamber and a more advanced hemispherical MESC chamber of the same size shows that a 20% improvement can be realized by using the more advanced design.

Further development effort should explore the use of a more advanced design MESC chamber and the performance impact of producing a larger chamber with a more favorable surface-to-volume ratio.

Acknowledgments

This work was supported by NASA Lewis Research Center under Contract NAS3-20393.

References

[1] Moore, R.D., "Magneto-Electrostatically Contained Ion Thruster," *AIAA Paper 69-260,* 7th Electric Propulsion Conference, Williamsburg, Va., March 1969.

[2] Ramsey, W., "12 Centimeter Magneto-Electrostatic Containment Mercury Ion Thruster Development," *Journal of Spacecraft and Rockets,* Vol. 9, May 1972, pp. 318-321.

[3] Sovey, J.S., "A 30-cm Diameter Argon Ion Source," NASA-TMX-73509, Lewis Research Center, Cleveland, Ohio, 1976.

[4] Mirtich, M.J., and Kerslake, W.R., "Long Lifetime Cathodes for 30-cm Mercury Thruster," NASA-TMX-73523, Lewis Research Center, Cleveland, Ohio, Nov. 1976.

[5] Aston, G., "The Ion-Optics of a Two-Grid Electron-Bombardment Thruster," NASA-CR-135034, May 1976.

[6] Dushman, S., *Scientific Foundations of Vacuum Techniques,* 2nd Ed., John Wiley & Sons, New York, 1962, p. 14.

[7] Byers, D.C. and Reader, P.D., "Operation of an Electron-Bombardment Ion Source Using Various Gases," NASA-TND-6620, Lewis Research Center, Dec. 1971.

[8] Strickfaden, W.D. and Geiler, K.L., "Probe Measurements of the Discharge in an Operating Electron-Bombardment Engine," *AIAA Journal,* Vol. 1, Aug. 1963, pp. 1815-1825.